LBNL-47275


ERNEST ORLANDO LAWRENCE
BERKELEY NATIONAL LABORATORY

# An Empirical Correlation for the Outside Convective Air Film Coefficient for Horizontal Roofs

R.D. Clear, L. Gartland and F.C. Winkelmann

**Environmental Energy Technologies Division**

January 2001

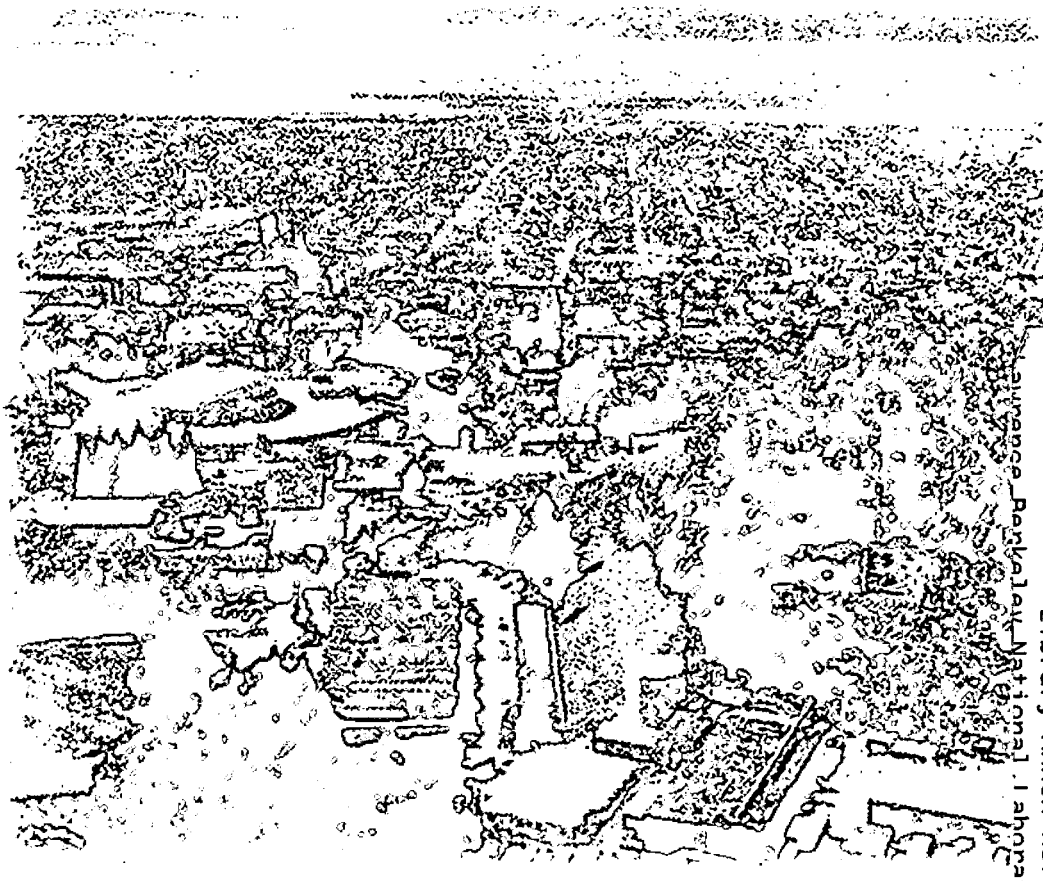

## DISCLAIMER

LBNL-47275

# An Empirical Correlation for the Outside Convective Air Film Coefficient for Horizontal Roofs

R. D. Clear, L. Gartland and F. C. Winkelmann

Environmental Energy Technologies Division
Lawrence Berkeley National Laboratory
Berkeley CA 94720-0001

January 2001

This work was supported by the Assistant Secretary for Energy Efficiency and Renewable Energy Office of Building Technology, State and Community Programs, Office of Building Research and Standards of the U.S. Dept. of Energy, under Contract No. DE-AC03-76SF00098.

# An Empirical Correlation for the Outside Convective Air Film Coefficient for Horizontal Roofs

R.D. Clear, L. Gartland[1] and F.C. Winkelmann
Environmental Energy Technologies Division
Lawrence Berkeley National Laboratory
Berkeley CA 94720

January 2001

## Abstract

From measurements of surface heat transfer on the roofs of two commercial buildings in Northern California we have developed a correlation that expresses the outside convective air film coefficient for flat, horizontal roofs as a function of surface-to-air temperature difference, wind speed, wind direction, roof size, and surface roughness. When used in hourly building energy analysis programs, this correlation is expected to give more accurate calculation of roof loads, which are sensitive to outside surface convection. In our analysis about 90% of the variance of the data was explained by a model that combined standard flat-plate equations for natural and forced convection and that took surface roughness into account. We give expressions for the convective air film coefficient (1) at an arbitrary point on a convex-shaped roof, for a given wind direction; (2) averaged over surface area for a given wind direction for a rectangular roof; and (3) averaged over surface area and wind direction for a rectangular roof.

## Introduction

Most commercial buildings have horizontal roofs. Heat flow through such roofs is sensitive to the outside convective air film coefficient, $h$, which is expected to depend on a number of factors, including wind speed and surface-to-air temperature difference. Particularly sensitive to $h$ is the fraction of solar radiation absorbed by the roof that is conducted into the building and appears as a cooling load. For this reason realistic values of $h$ are needed to accurately calculate cooling requirements.

The value of $h$ currently used for roofs in hourly building energy simulation programs is based on comparisons determined from measurements under laboratory conditions on surface samples orders of magnitude smaller than typical roof dimensions. To eliminate the uncertainty in scaling such correlations to full-sized surfaces, we have measured $h$ for the roofs of two commercial buildings in Northern California and, from fits to the measurements, have extracted a correlation for $h$ in terms of wind speed, roof-to-air temperature difference, roof size, and surface roughness. Our correlation complements similar comparisons that have been established for vertical building surfaces (see [YA94], which describes a correlation for windows and summarizes related work on exterior vertical-surface film coefficients).

## What Was Measured

The results are based on heat transfer data that were collected as part of the Cool Roofs Project [KO98] to determine the effect of higher roof reflectance on air-conditioning loads. This project examined three different one-story commercial buildings in the Northern California cities of Davis, San Jose and Gilroy (because of limited access to the roof in the Gilroy building, only the Davis and San Jose data were used to determine $h$). Figure 1a shows a ground-level view of the Davis building. The buildings have flat, horizontal, built-up asphalt capsheet roofs. Figure 1b shows the roof of the Davis building (the San Jose building's roof is similar). Table 1 gives some geometrical information about the roofs.

[1] Now at PositivEnergy, 397 51st Street, Oakland, CA 94609

## NOMENCLATURE

| | |
|---|---|
| $A$ | roof surface area [$m^2$] |
| $E$ | laminar flow correction factor |
| $Gr_{L_n}$ | Grashof number, $g\rho^2 L_n^3 \Delta T/(T_f \mu^2)$ |
| $g$ | gravitational constant [9.81 $m/s^2$] |
| $h$ | surface convection coefficient [$W/m^2$-K] |
| $h_n$ | flat-plate natural convection coefficient [$W/m^2$-K] |
| $h_f$ | flat-plate forced convection coefficient [$W/m^2$-K] |
| $k$ | conductivity of air [W/m-K] |
| $l$ | $4A/P$ [m] |
| $L$ | strip length [m] |
| $L_{eff}$ | effective length for forced convection [m] |
| $L_n$ | characteristic length for natural convection (area-to-perimeter ratio) [m] |
| $L_{max}$ | maximum lineal dimension [m] |
| $Nu$ | Nusselt number |
| $P$ | Perimeter [m] |
| $Pr$ | Prandtl number, $\mu/(\rho\alpha)$ |
| $Q_{solar}$ | solar radiation absorbed by roof [$W/m^2$] |
| $Q_{sky}$ | sky long-wave radiation absorbed by roof [$W/m^2$] |
| $Q_{cond}$ | conductive heat flow into roof [$W/m^2$] |
| $Q_{IR}$ | long-wave radiation emitted by roof [$W/m^2$] |
| $Q_{net}$ | $Q_{solar}+Q_{cond}-Q_{IR}$ [$W/m^2$] |
| $Ra$ | Rayleigh number, $GrPr$ |
| $Re_x$ | Reynolds number, $w\rho x/\mu$ |
| $R_f$ | surface roughness factor |
| $r$ | rectangle length-to-width ratio |
| $S_i$ | temperature factor for condensation calculation [K] |
| $s$ | ratio of critical length to circle diameter |
| $t$ | $4A^{1/2}/P$ |
| $T_f$ | roof surface film temperature—average of roof temperature and outside air temperature [K] |
| $T_r$ | roof outside surface temperature [K] |
| $T_d$ | outside air dewpoint temperature [K] |
| $x$ | distance along wind direction from roof edge to convection coefficient evaluation point [m] |
| $x_c$ | critical length (length of laminar region for forced convection) [m] |
| $W$ | rectangle width [m] |
| $w$ | free-stream wind speed at roof level [m/s] |

**Greek symbols**

| | |
|---|---|
| $\alpha$ | thermal diffusivity of air evaluated at $T_f$ [$m^2/s$] |
| $\Delta T$ | roof outside surface temperature minus outside air temperature [K] |
| $\eta$ | weighting factor for natural convection |
| $\mu$ | viscosity of air evaluated at $T_f$ [N-s/$m^2$] |
| $\rho$ | density of air evaluated at $T_f$ [$kg/m^3$] |

**Subscripts**

| | |
|---|---|
| $c$ | critical |
| *center* | center of roof or roof section |
| *eff* | effective |
| $f$ | forced convection |
| *fit* | fitted |
| *lam* | laminar flow |
| *meas* | measured |
| $n$ | natural convection |
| *turb* | turbulent flow |

**Table 1: Roof Dimensions and Characteristic Lengths**

| Site | Area ($m^2$) | Perimeter (m) | Characteristic Length (m)* | |
|---|---|---|---|---|
| | | | Forced Convection | Natural Convection |
| Davis, CA | 2940 | 287 | 28.3 | 10.2 |
| San Jose, CA | 2370 | 195 | 27.3 | 12.1 |

*The characteristic length for forced convection is defined as the average distance from the roof perimeter to the heat transfer measurement point. The characteristic length for natural convection is defined as the area-to-perimeter ratio.

**Figure 1(a): Ground-level view of the Davis building**

Data were collected at 15-minute intervals for over a year at each location. The measured quantities used to determine $h$ were

- roof outside surface temperature
- roof conductive heat flow
- outside air temperature
- outside air humidity
- wind speed
- total (direct plus diffuse) horizontal solar radiation
- roof solar absorptance
- roof dimensions

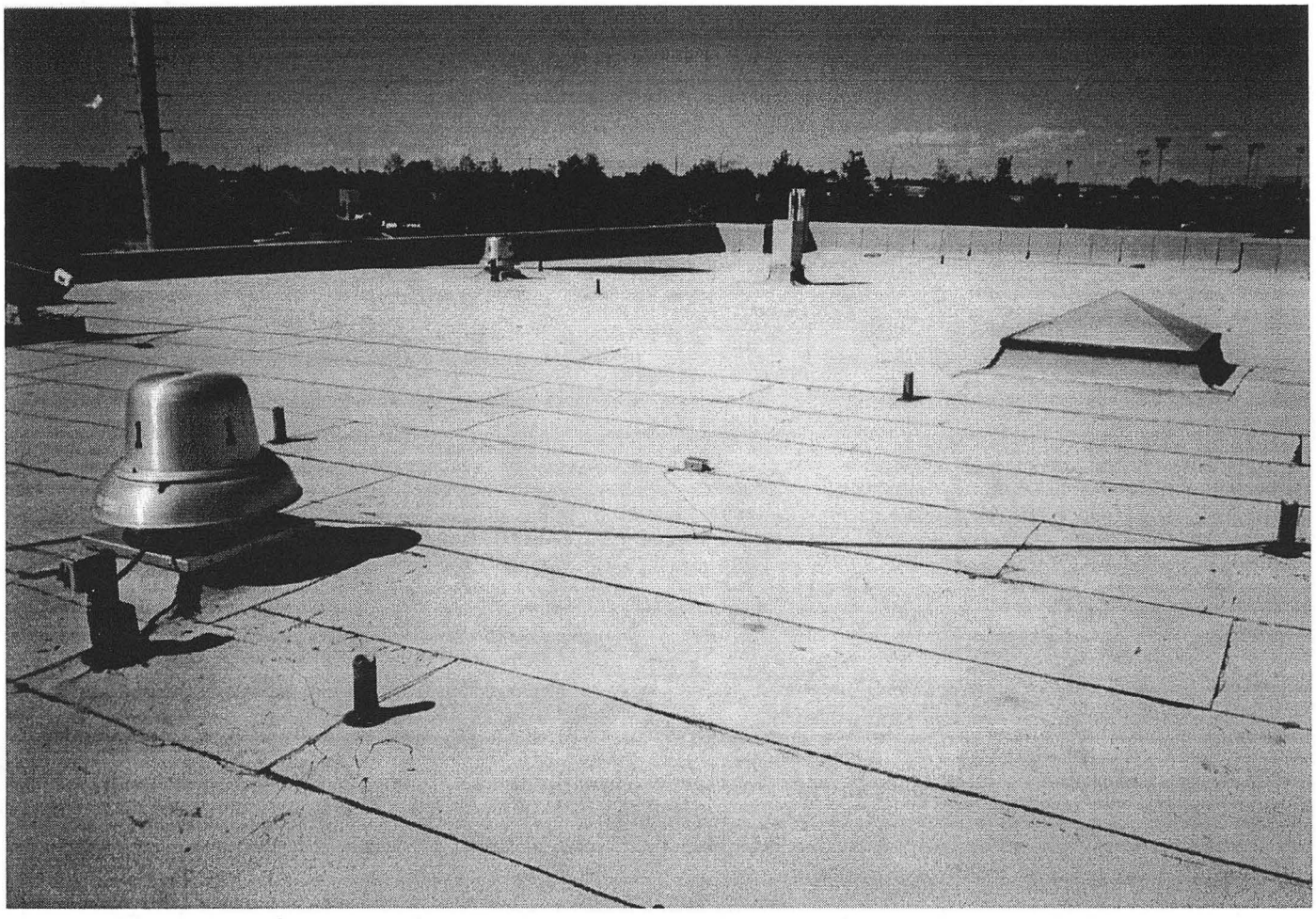

**Figure 1(b): Roof of the Davis building.**

The accuracy of these measurements is summarized in Table 2. Other measurements that were made, but not used in the *h* analysis, were wind direction, roof inside surface temperature, plenum air temperature, return air temperature, inside air temperature and air-conditioning energy use.

**Table 2: Measurement accuracy.**

| Variable | Sensor type | Measurement accuracy |
|---|---|---|
| Roof surface temperature (C) | Platinum RTD, transmitter | ±0.3C |
| Roof conduction ($W/m^2$) | Thermopile flux meter | ±3 $W/m^2$ |
| Outside air temperature (C) | Platinum RTD | ±0.3C |
| Wind speed (m/s) | Three-cup anemometer | ±0.25 m/s ( < 5 m/s)<br>±5% ( > 5 m/s) |
| Horizontal insolation ($W/m^2$) | Silicon pyranometer | ±3% |
| Relative humidity (%) | Capacitive RH sensor | ±2% (0-90% RH)<br>±3% (90-100% RH) |

Thermal and meteorological measurements were made at a single point at the approximate center of each roof. The meteorological station was 3m above the roof (which, in turn, was about 5m above ground level). The conductive heat flow was measured with a thermopile thermal flux transducer located just below the roof's outside surface layer. The

surface temperature was measured with a platinum resistive device located adjacent to the heat flux transducer at the same depth. The solar absorptance, measured as the ratio of the readings of a pyranometer facing toward and away from the roof on a clear day with the sun high in the sky, was 0.76±0.03 in Davis and 0.84±0.03 in San Jose. Although data were also taken after a white coating was applied to the roofs, our analysis was restricted to the uncoated data because of the larger range of temperature difference between roof surface and outside air.

The capsheet roofing consists of 1.2m x 3m rectangular sections and has a construction similar to residential asphalt roofing shingles, with surface granules pressed into asphalt-saturated fibers. The capsheet thermal emissivity was estimated to be 0.9, which is typical of the surface granules.

Because the Cool Roofs Project was not designed to measure the roof surface heat transfer coefficient, we were only able to analyze a fraction of the data. Table 3 lists the range of the variables for the data set as a whole and for the subset of the data that we actually analyzed. For reasons that are discussed later, the data that were kept were restricted mostly to daytime periods under clear skies. The average temperatures and insolation values are therefore considerably higher for the data that was analyzed than for the full data set.

**Table 3: Average value and range of key measured variables.**

| **Full data set: 49,630 points** | | | |
|---|---|---|---|
| **Variable** | **Range** | **Average** | **Standard deviation** |
| Roof surface temperature (C) | -12 to 81 | 20 | 19 |
| Surface-to-air temperature difference (K) | -14 to 87 | 4.4 | 13.2 |
| Outside air temperature (C) | -12 to 42 | 16 | 7.3 |
| Wind speed (m/s) | 0 to 9.3 | 1.4 | 1.2 |
| Horizontal insolation ($W/m^2$) | 0 to 1026 | 177 | 264 |
| Relative humidity (%) | 9 to 104* | 64 | 23 |
| Roof conduction ($W/m^2$) | -261 to 283 | -1.7 | 36 |
| **Subset analyzed: 7979 points** | | | |
| **Variable** | **Range** | **Average** | **Standard deviation** |
| Roof surface temperature (C) | 2 to 79 | 46 | 16 |
| Surface-to-air temperature difference (K) | 0 to 49 | 22 | 12 |
| Outside air temperature (C) | 1 to 41 | 24 | 7.2 |
| Wind speed (m/s) | 0 to 9.3 | 1.9 | 1.4 |
| Horizontal insolation ($W/m^2$) | 0 to 1003 | 535 | 244 |
| Relative humidity (%) | 9 to 102* | 36 | 14 |
| Roof conduction ($W/m^2$) | -261 to 207 | 7 | 55 |

*Measured relative humidity at night sometimes slightly exceeded saturation (100% relative humidity). Most of the nighttime data were not included in the subset of the data that was analyzed, and there were only four data points in this set that exceeded 100%. No correction was made for these four points since they affect the calculated heat flows by less than 0.1% and do not significantly add to the error in the calculated convection flows.

## Roof Surface Heat Balance

The roof surface heat balance equation used to extract $h$ is

$$Q_{solar} + Q_{sky} + Q_{cond} - Q_{IR} - h\Delta T = 0 \quad (1)$$

where $h\Delta T$ is the convective heat transfer from the roof to the outside air ($W/m^2$).

$Q_{solar}$ and $Q_{cond}$ were directly measured. $Q_{IR}$ was calculated from the measured roof temperature and the assumed roof emissivity. $Q_{sky}$ was inferred from empirical correlations [WA83, MA84, BR97] that give sky emissivity (or sky temperature) in terms of air temperature and humidity. $\Delta T$ was calculated from the measured roof surface temperature and measured air temperature.

## Statistical Analysis Considerations

The convective air film coefficient was assumed to be a function of a natural convection coefficient, $h_n$, and a forced convection coefficient, $h_f$; i.e.,

$$h = f\left(h_n, h_f\right)$$

The form chosen for this function is described in "Surface Convection Models," below.

We expect errors in the measured quantities to be independent of $\Delta T$ and it is therefore appropriate to fit the quantity $f(h_n,h_f)\Delta T$ to the measurements to determine $h$. The alternative of dividing by $\Delta T$ to directly fit $f(h_n,h_f)$ produces errors that are potentially unbounded as $\Delta T \rightarrow 0$.

Another important issue that was encountered in doing the fits was how to deal with the $Q_{sky}$ term. The commonly-used sky emissivity formulas from Walton [WA83], Martin and Berdahl [MA84], and Brown [BR97] produce estimates that are displaced from each other and have different slopes vs. ambient dewpoint temperature (Fig. 2). Errors from the estimate of $Q_{sky}$ are not random errors, so the estimate must be treated as an independent variable. We assume that a reasonable model for $Q_{sky}$ has the form

$$Q_{sky,true} = A + BQ_{sky,estimate} + \text{ random error} \tag{2}$$

From Eq. 1, this leads to the following form for the fits:

$$Q_{solar} + Q_{cond} - Q_{IR} = f\left(h_n, h_f\right)\Delta T - \left(A + BQ_{sky}\right) \tag{3}$$

The goal was to find what values of the parameters on the right-hand side of this equation—i.e., the values of $A$ and $B$, and of the parameters in the expression for $f$—that give the best least-squares fit to data values on the left-hand side of the equation. Here, $Q_{sky}$ is given by one of the three sky models and the fitted values of $A$ and $B$ depend on which model is used.

Fitting one month of data at a time for both San Jose and Davis showed no relationship between $A$ or $B$ for Davis vs. San Jose, and showed that these values varied from month to month. Combining the monthly data and doing annual fits showed that $A$ tended to zero and $B$ to 1, but using these average values gave poor monthly fits. Furthermore, we noted that the parameters for $f(h_n,h_f)$ were fairly stable when $A$ and $B$ were allowed to vary monthly, but were unstable and often had nonsense values when $A$ and $B$ were fixed. The main problem was that allowing monthly variation in $A$ and $B$ led to a large number of free parameters when the monthly data were combined. However, we found that it was possible to use a single value of $A$ as long as $B$ varied monthly or vice versa. This is the procedure that was used since it resulted in only a small loss in the degree of fit and almost no change in the estimates of the parameters for $f(h_n,h_f)$. A possible reason for the time dependence of $A$ or $B$ was variation in atmospheric turbidity, which none of the sky models account for.

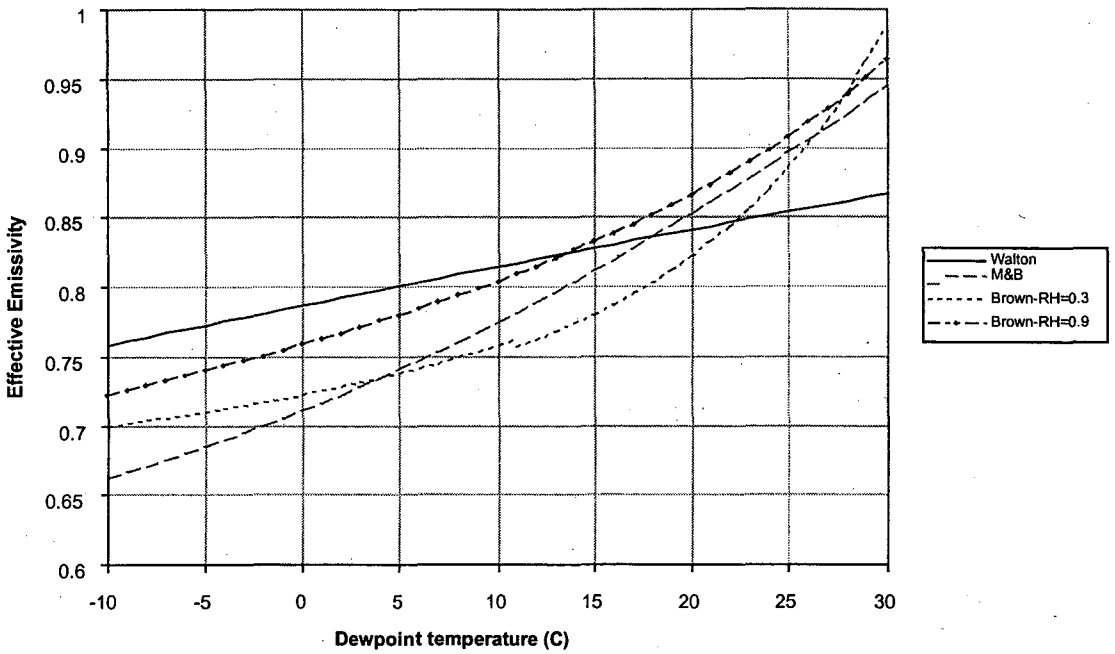


**Figure 2: Clear sky emissivity vs. dewpoint temperature as predicted by the Walton, Martin and Berdahl, and Brown models. Two values of relative humidity are shown for the Brown model.**

## Data Cleaning and Adjustment

The data collection period ran from July 1996 to February 1997 in San Jose and from July 1996 to March 1997 in Davis. Before cleaning there were about 25,000 data points from each site. The July 1996 Davis data was one of the best data sets for analysis and was used in a number of figures in this paper to illustrate the analysis.

Figure 3 shows a plot of the raw values of $h\Delta T$ versus $\Delta T$ for this month. In this figure $h\Delta T$ was determined from Eqs. 1 and 2 with the Walton sky model with default values of $A = 0$ and $B = 1$. We note from the plot that $h\Delta T$ increases with $\Delta T$ when $\Delta T > 0$, as expected. However, for $\Delta T < 0$, $h\Delta T$ also increases when $|\Delta T|$ increases, which is unphysical. We also note that the centroid of the distribution as a function of $\Delta T$ does not go through (0,0), which it must if we are estimating $h\Delta T$ correctly. These are symptoms of physical problems that affected the raw data, and which required extensive pruning and some adjustment before it could be used for analysis. After this data cleaning there remained 3373 data points for San Jose and 4612 data points for Davis.

Several types of cleaning were applied to the data. Data points were eliminated if there was missing information or anomalous values. This was particularly true for the wind speed data. Data that couldn't be modeled properly were also eliminated. As described in the following sections, this eliminated cloudy days, periods where there might be condensation on the roof, and periods where the roof temperature was lower than the air temperature. We also made two adjustments to the data: the measured solar absorptance was adjusted for changes in roof surface specularity as a function of the angle of incidence of radiation, and the measured roof temperatures and conductive heat flows were adjusted for time-lag effects between the roof surface and the sensors, which were located below the capsheet.

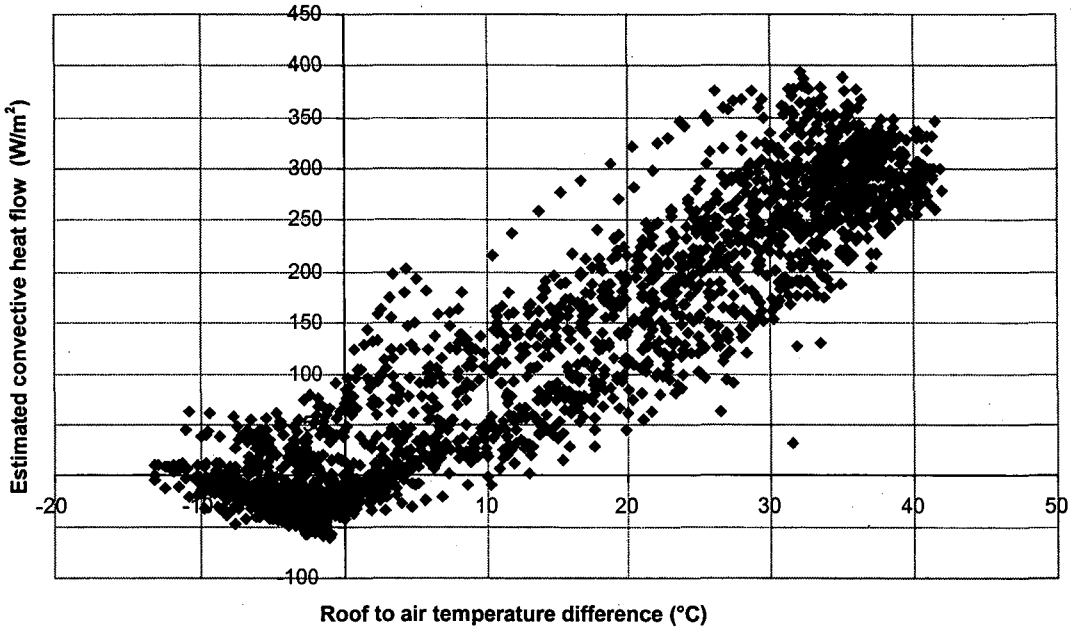


**Figure 3: Estimated convective heat flux at roof center *vs.* surface-to-air temperature difference for a representative sample of raw data (July 1996, Davis).**

### *Elimination of cloudy days*

We eliminated cloudy days so that the sky emissivity models, which are most accurate for clear skies, could be applied. Clear days were identified from the ratio of measured solar radiation to calculated clear sky solar radiation. Figure 4 shows an example of the ratios for the first half of March in Davis. Ratios greater than 1.0 were reset to 1.0. Days were considered to be clear if, from visual examination, most of the hours had ratios close to or above 1.0. These days are indicated in the figure. Among the reasons for visual screening was that ratios early in the morning and late in the evening were less accurate than during the middle of the day because they were much more sensitive to small inaccuracies in the calculated values, and were also constrained by the precision and accuracy of the measuring equipment. Early morning data was also more likely to be rejected because of other problems, such as the potential for condensation on the roof. Another issue was that a small cloud between the sun and the measurement point made a large, but temporary, change in the ratio without making much difference to the sky radiation computation. Thus, we wanted to ignore isolated dips in the ratio, whereas repeated dips indicated more extensive cloud cover. As a general rule, days were considered to be clear only if the ratio for the whole day was about 0.9 or above and the standard deviation of the ratios during the day was less than about 0.1. Days with higher average ratios or lower standard deviations were sometimes eliminated if these occurred in the middle of the day or if there appeared to be a pattern indicating the presence of many clouds.

### *Elimination of cases with condensation*

Equation 1 does not have a term for moisture condensation or evaporation, which we have not modeled. Therefore we removed time periods with the potential for condensation and/or evaporation. We assumed that condensation occurred when the roof temperature, $T_r$, was below the calculated dew-point temperature, $T_d$. We further assumed that the amount of condensate during any period was proportional to $T_r$-$T_d$. This led to the following algorithm to exclude condensation/evaporation:

(1) Start during a period when no condensation is expected and set $S_0 = 0$.

(2) For period $i$, if $S_{i-1} < 0$ or $T_r - T_d < 0$, then $S_i = S_{i-1} + T_r - T_d$ ; else $S_i = 0$.

(3) Exclude all periods with $S_i < 0$ as having potential condensate.

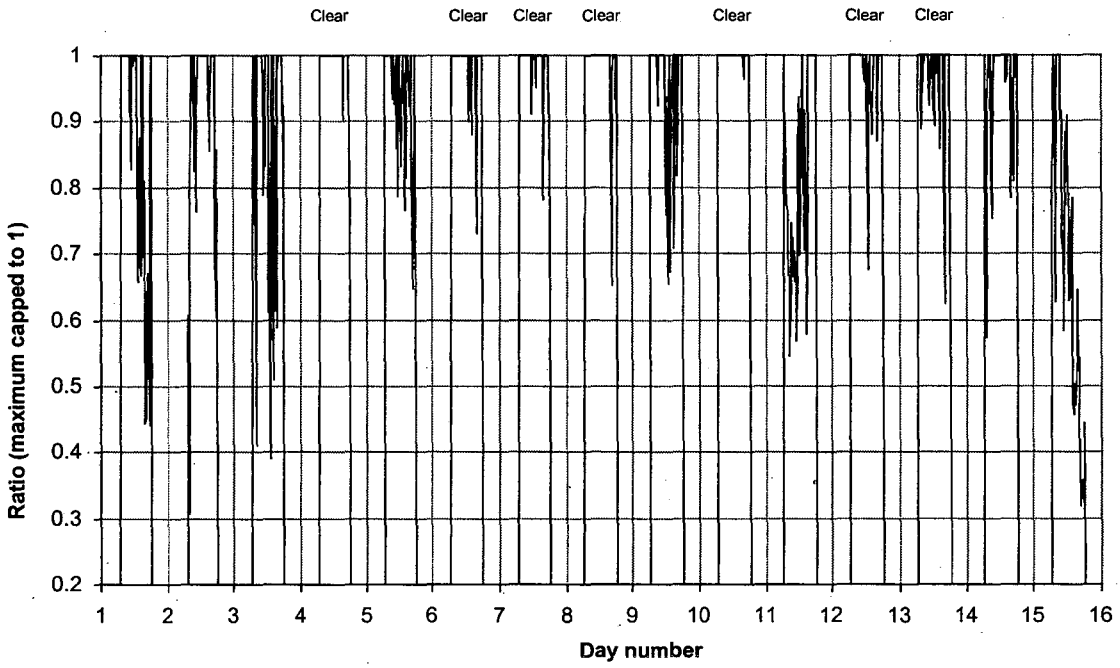


**Figure 4: Ratio of measured to calculated total horizontal solar irradiance for March 1997 in Davis. Values greater than 1.0 have been set to 1.0.**

### *Removal of anomalous wind speeds*

The wind speed monitor occasionally reported an error condition and would sometimes report zero wind speeds in the middle of a period of fairly high wind speeds. Figure 5 shows wind speed vs. wind speed in the previous time interval for the July 1996 Davis data. We see that wind speeds are generally fairly well correlated from time step to time step. The points on the zero wind speed axes extend out past the pattern of correlation for non-zero wind speed data and are therefore almost certainly due to an error condition.

Because there is a high degree of auto-correlation between points, interpolated wind speeds were used in place of isolated errors, but data were excluded if there were several consecutive points missing. Zeros were left as zeros when they occurred in the middle of a run of low values. Zeros that occurred in the middle of a run of high values were treated as error values.

Figure 6 shows the same data as in Fig. 3 but after performing the cleaning just described, i.e., removing cloudy days and removing data points with condensation or anomalous wind speed. Cleaning reduced the spread in the data for $\Delta T < 0$, accentuating the fact that the distribution does not pass through (0,0). This problem is addressed in the next section.

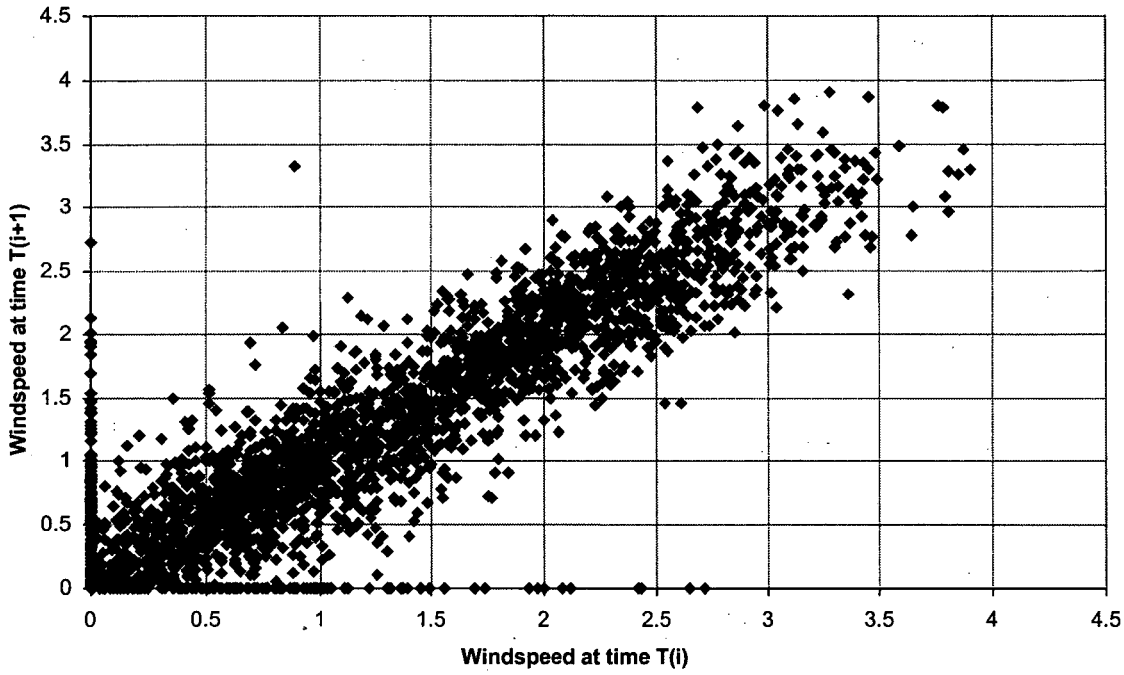


**Figure 5: Temporal correlation of wind speeds in Davis for July 1996. For each point, the horizontal axis gives the wind speed at a particular time and the vertical axis gives the wind speed at the next measurement time (15 minutes later).**

### *Correction for time-lag effects*

The roof temperature and heat flux sensors were located under the capsheet, 3.9 mm below the roof surface. To get the actual surface temperature and flux a correction was made to the measured temperature and flux to account for the conductive time lag across the capsheet. The properties of the capsheet material used to make this correction are given in Table 4.

**Table 4: Capsheet material properties.**

| | |
|---|---|
| Thickness | 0.0039 m |
| Conductivity | 0.144 W/m-K |
| Density | 1120 kg/m$^3$ |
| Heat Capacity | 1510 J/kg-K |
| Diffusivity | 8.5x10$^{-8}$ m$^2$/s |

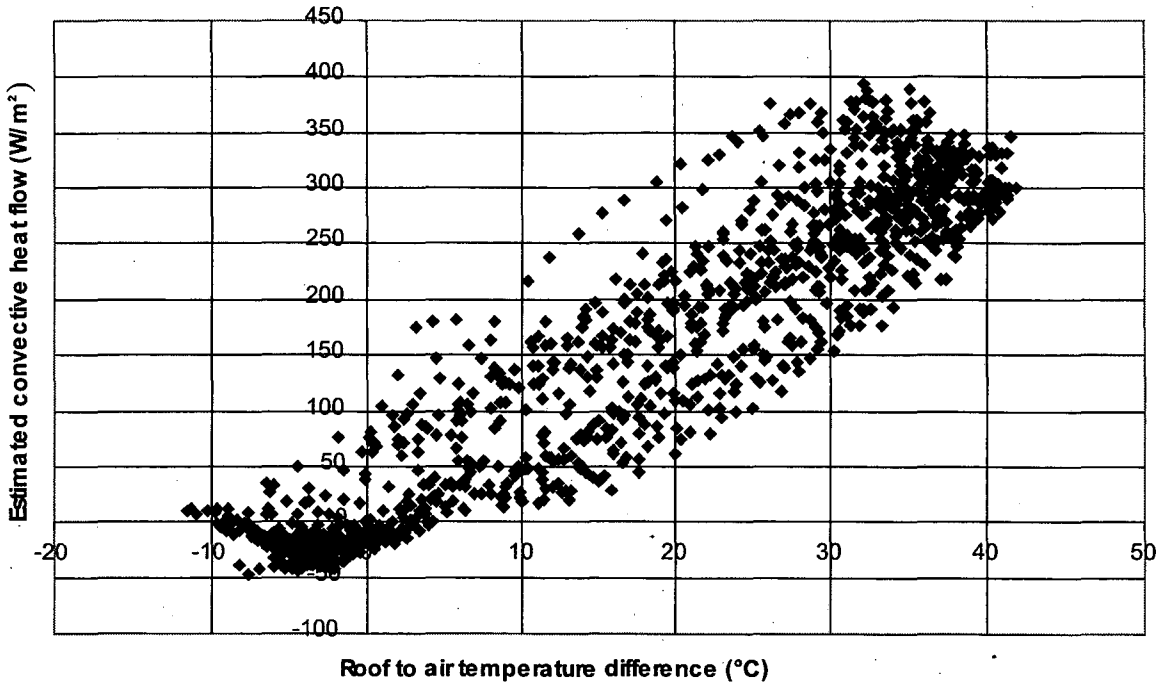


**Figure 6: Measured convective heat flux at roof center *vs* surface-to-air temperature difference for a representative sample of data (July 1996, Davis) with cloudy days and condensation conditions removed.**

To compute the surface heat flow we assumed that the roof acted like a semi-infinite slab. The heat flow solution, taken from Carslaw and Jaeger [CA59], was used to determine the surface temperature and flux from the measured subsurface temperature and flux. The average temperature adjustment was about 0.1K with maximum deviation of about 6K (±2%). The average heat flux adjustment was about 0.3 W/m$^2$, with maximum deviations up to 100 W/m$^2$ in mid-morning or afternoon or when a cloud suddenly obscures the sun. In the later case the adjusted heat flux first goes substantially lower than the measured flux, and then goes substantially higher, before finally settling down to approximately the same value.

Figure 7 shows $h\Delta T$ vs $\Delta T$ with the lag correction. The adjusted distribution passes through (0,0), as required, and echoes the timing of changes in the solar heat gain, while the unadjusted values (Fig. 6) lag and do not pass through (0,0).

In Fig. 6 there are a substantial number of points for which $h\Delta T$ is opposite in sign to the temperature gradient, $\Delta T$. For $\Delta T > 0$ the lag corrections that were applied in Fig. 7 eliminated about 90% of these anomalies and reduced the magnitude of those that remain. As discussed in the next section, the remaining anomalies, including those for $\Delta T > 0$, are probably due to small errors in the estimate of the long-wave sky radiation.

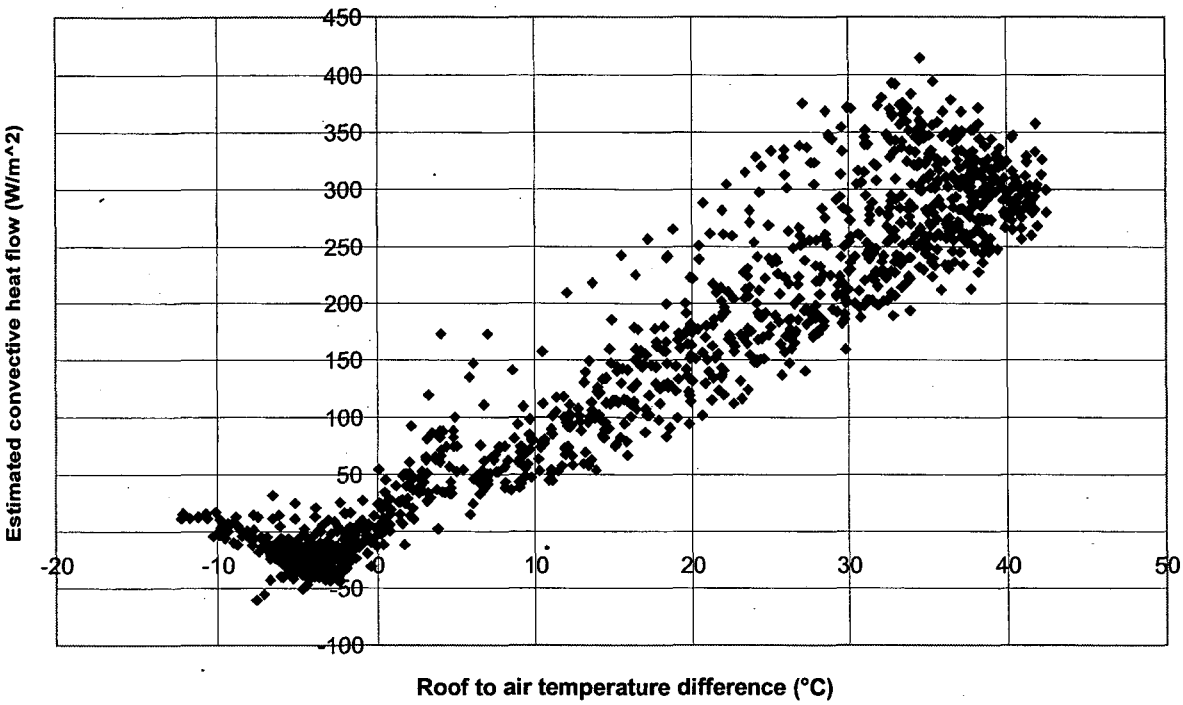


**Figure 7: Measured convective heat flux at roof center *vs* surface-to-air temperature difference for a representative sample of data (July 1996, Davis) with cloudy days and condensation conditions removed, and corrected for conduction time lag between sensor location and roof surface.**

***Elimination of cases with roof temperature below air temperature***

We removed all data with $\Delta T < 0$, i.e., roof temperature less than outside air temperature. This exclusion was, like the non-clear sky exclusion, due to our reliance on a $Q_{sky}$ estimation. The roof temperature can fall below the air temperature at night or early in the morning for the clear, dry conditions that are common in Davis and San Jose. When this happens the long-wave radiative loss from the roof dominates: it is typically 10 times or more higher than the convective and conductive heat transfer. Under these conditions a small percentage error in $Q_{sky}$ can lead to large and systematic errors in $h\Delta T$, as shown in Fig. 7. In this figure the parameters $A$ and $B$ of Eq. 3 were set to the default values of 0 and 1, respectively. The lowest $\Delta T$ values show an estimated convective heat flow that is opposite to the temperature gradient. This implies an error in $Q_{sky}$ since this is the only term of sufficient magnitude and uncertainty to produce this anomalous effect.

There are no obvious problems in the data for $\Delta T > 0$. At night and during late morning or early evening, $\Delta T > 0$ implies that the real $Q_{sky}$ is equal to or greater than the estimated value. The estimated sky emissivity for the algorithms we used for the San Jose and Davis clear sky conditions ranges from about 0.7 to 0.85, with an average of about 0.8. It is physically unlikely for the emissivity to be much higher than these values for clear sky conditions. This limits the likelihood that the estimated convective heat flow will be significantly lower than the true value at the highest $\Delta T$ values.

Sky radiation models estimate the sky emissivity from the ambient air temperature and humidity. If the sky emissivity is high, then ground (and roof) temperature will also tend to be high because of the increased long-wave radiation from the sky. When the ground temperature is higher than the air temperature the convective coupling between ground and air is fairly high. This makes the ambient air temperature more closely related to the sky

radiation level and should reduce the size of potential underestimates of the sky radiation term. When $\Delta T < 0$ the convective coupling between ground and air is lower and, thus, the potential for overestimation of the sky radiation term from the air temperature is large.

During the day the absorbed solar radiation becomes the dominant heat flow term, with the long-wave roof radiation term dropping to second, and the convective term rising to become comparable to the long-wave sky radiation term. As a consequence errors in the estimation of $Q_{sky}$ are less important.

Equally important during the day is that the sun drives the magnitude of $\Delta T$. If the sky is more, or less, transparent to solar radiation than normal, there should be an increase, or decrease, in the solar gain term, and an (at least) partially compensating decrease, or increase, in the long-wave $Q_{sky}$ term. Therefore, errors in the estimation of $Q_{sky}$ should have little correlation with the overall magnitude of the total radiation heat input (sky and solar) and thus little correlation with $\Delta T$. This means that there should be little or no bias error in our estimation of the convection coefficient due to a correlation of an error in our estimation of the $Q_{sky}$ and $\Delta T$ during daytime conditions where $\Delta T > 0$.

***Adjustment of solar absorptance for angular effects***

The capsheet material reflects more sunlight at grazing angles than at normal incidence. An estimate of the magnitude of this effect was made by assuming a capsheet index of refraction of 1.4. The incident solar radiation was partitioned into beam and sky components using Schulze's formula [SC70]. The reflectance of the sky component was estimated from a numerical integration over the radiance of the sky as a function of sky angle using the Kittler clear sky radiance formula [CI73]. The resulting correction factor to the roof solar absorptance ranged from 1.0 at the reference measurement condition (high solar altitude) to 0.9 at 20° solar altitude to 0.75 at 0° solar altitude.

## Plots of measured *h* values

Figures 8 through 10 are plots of measured values of $h$ for cleaned and adjusted data for the same one-month time period and location (July 1996, Davis) shown in Fig. 7. The values of $h$ that are shown were calculated from Eq. 1 using fitted $Q_{sky}$ values.

Figure 8 shows $h$ vs time. Non-clear days and condensation conditions are excluded, but the figure does include cases with $\Delta T < 0$. When $\Delta T$ approaches zero, small errors in heat flow translate into large errors in $h$. This appears in the figure as very high, and occasionally very low, $h$ values at the beginning and end of the day and at the night. (In Figs. 8, 9 and 10, a small number of points with $h < -20$ or $> 40$ were not plotted to avoid losing detail in the remaining data.) During the day $h$ generally increases during the morning to a mid-afternoon peak, then declines. This pattern reflects the $\Delta T$ and wind speed patterns at the site.

Figure 9 shows $h$ vs. $\Delta T$. The dependence on $\Delta T$ is fairly weak and we see the loss in precision as $\Delta T$ approaches zero.

Figure 10 shows $h$ vs. wind speed. The dependence on wind speed is slightly sub-linear.

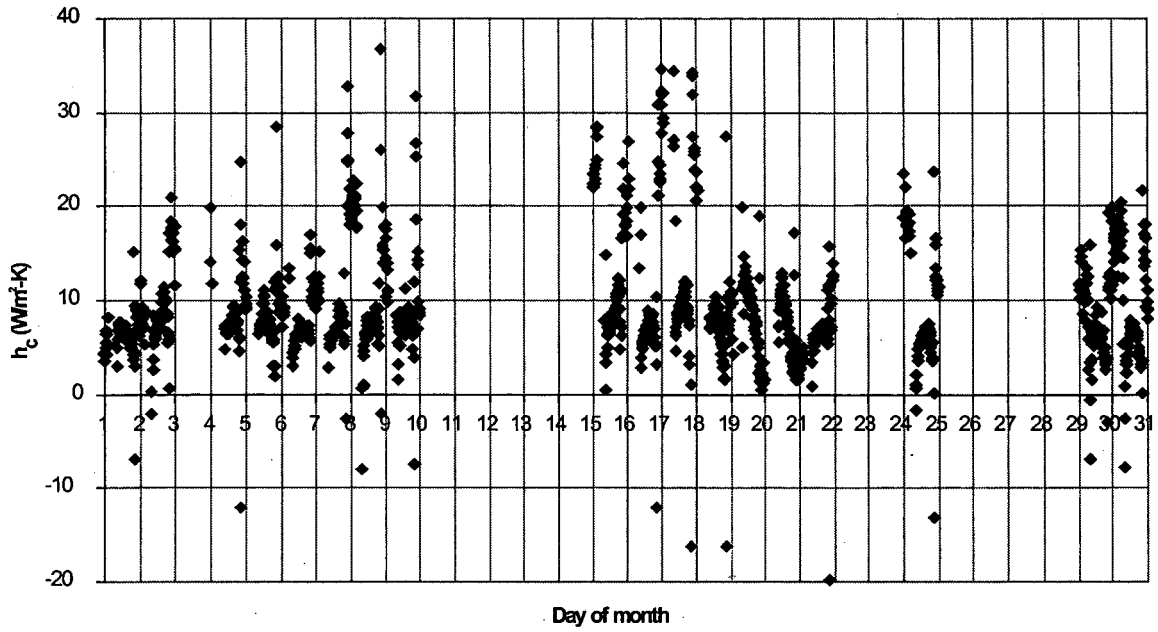


**Figure 8: Measured convective heat transfer coefficient at roof center *vs* time for the data shown in Fig. 7.**

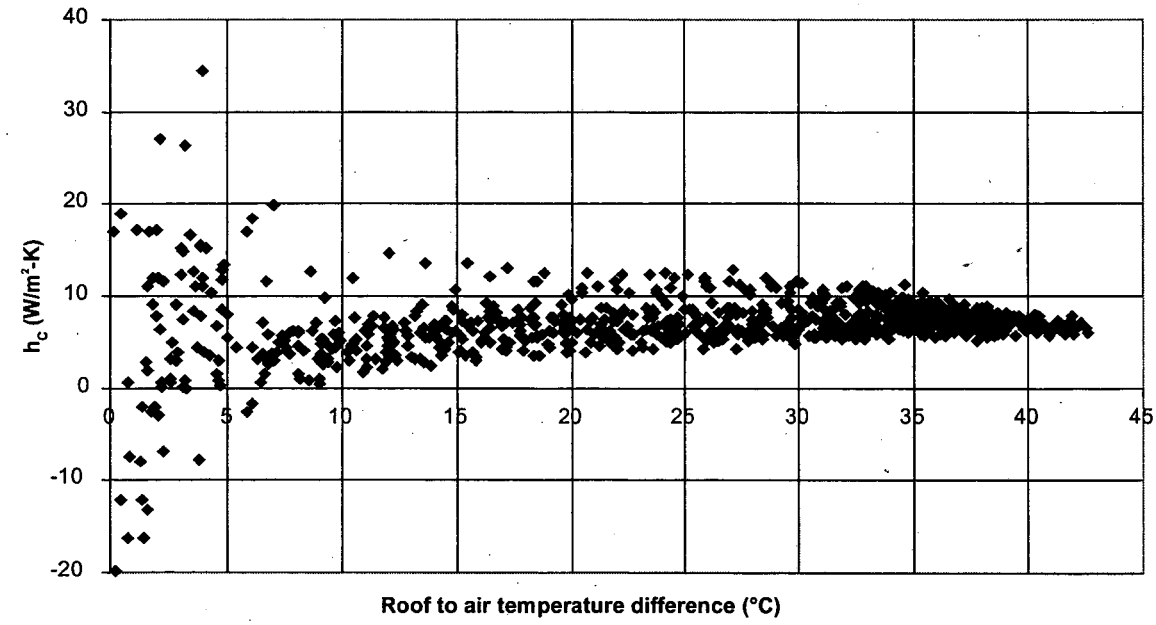


**Figure 9: Measured convective heat transfer coefficient at roof center *vs* surface-to-air temperature difference for the data shown in Fig. 7.**

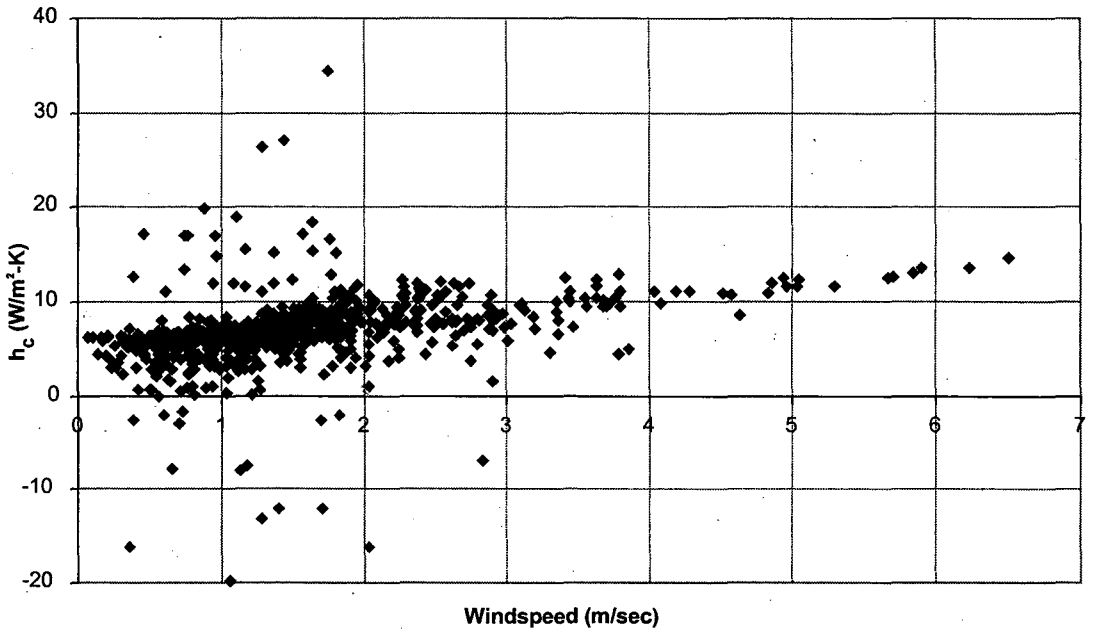


**Figure 10: Measured convective heat transfer at roof center *vs* wind speed for the data shown in Fig. 7.**

## Surface Convection Models

Model fitting was based on standard convection heat flow correlations (shown in Table 5) that have been derived for flow over smooth horizontal isothermal flat plates with the upper surface heated [IN96].

**Table 5: Convective Heat Flow Correlations**

| Type of convection | Applicable range | Nusselt number (*Nu*) |
|---|---|---|
| Natural | $\Delta T > 0$, $Ra < 10^7$ (Laminar) | $0.54Ra^{1/4}$ |
| | $\Delta T > 0$, $10^7 < Ra < 10^{10}$ (Turbulent) | $0.15Ra^{1/3}$ |
| | $\Delta T < 0$, $10^5 < Ra < 10^{10}$ | $0.27Ra^{1/4}$ |
| Forced | $Re < 10^5$ (Laminar) | $0.332\,\mathrm{Re}_x^{1/2}\,\mathrm{Pr}^{1/3}$ |
| | $10^5 < Re < 10^8$ (Turbulent) | $0.0296\,\mathrm{Re}_x^{4/5}\,\mathrm{Pr}^{1/3}$ |

For forced convection, $x$ in this table is the distance from the leading edge of the plate to the point at which the Reynolds number is evaluated.

Because of the size of the roofs, *Ra* at the measurement point always exceeded the range for laminar natural convection for $\Delta T > 0$ and, in fact, often exceeded by a factor of 100 or more the recommended range of the equation for turbulent natural convection. *Re* is proportional to wind speed, and there were a substantial number of low wind speed points (< 0.1 m/s) that gave *Re* values that were nominally in the laminar flow region. However, the fits to the data were almost always better if the flow was assumed to be turbulent. In retrospect, it seems likely that any time natural convection is turbulent, then the mixed natural/forced convection should be turbulent also. All of our fits are based on turbulent flow at the measurement point for both the natural and forced convection conditions.

The relative importance of natural and forced convection is related to the quantity $Gr/Re^2$ (where $Gr$ is the Grashof number), which is a measure of the ratio of buoyancy forces to inertial forces [IN96]. Natural convection is expected to dominate when $Gr/Re^2 >> 1$ and forced convection is expected to dominate when $Gr/Re^2 << 1$. Natural and forced convection are expected to be of roughly equal importance when $Gr/Re^2 \approx 1$, but there is little guidance in the literature on how to combine natural and forced convection in this case. The most obvious way to combine them was to simply add the terms. Alternatively, it seemed likely that when one term was dominant, the other would be suppressed. Initial fits did not support suppression of forced convection when natural convection dominated, but did provide some support for suppression of natural convection when forced convection dominated.

After consideration of a number of possibilities, the following two functions were chosen for fitting[2] the whole data set since they gave good and relatively stable fits over the different months in the data sets; they also gave rapid convergence. (None of the data showed any correlation with wind direction, so this was not included in any of the fits.)

$$f_1(h_n, h_f)\Delta T = \left[Ch_n + Dh_f\right]\Delta T \tag{4a}$$

$$f_2(h_n, h_f)\Delta T = \left[\eta Ch_n + Dh_f\right]\Delta T \tag{4b}$$

where

$$\eta = \frac{\ln(1 + Gr_x / \mathrm{Re}_x^2)}{1 + \ln(1 + Gr_x / \mathrm{Re}_x^2)}$$

and $x$ is the distance along the wind direction between the point that the wind hits the edge of the roof and the measurement point. The quantities $h_n$ and $h_f$ are the flat-plate natural and forced convection coefficients, respectively, obtained from the Nusselt numbers in Table 5, and $C$ and $D$ are fitted constants.

In Eq. 4a we are assuming that natural and forced convection are additive and the flat-plate correlations for convection are valid to within scale factors ($C$ and $D$) under all conditions. If the flat-plate correlations are exactly correct for roofs and natural and forced convection are indeed additive, then $C$ and $D$ in Eq. 4a will both equal 1.0.

In Eq. 4b we also assume that natural and forced convection are additive, but that natural convection is suppressed when forced convection is large ($\eta \rightarrow 0$ as the Reynolds number becomes large). C and D in Eq. 4b will again equal 1.0 if the flat-plate correlations apply exactly to the roof situation in the limit of pure natural convection or pure forced convection. Of course, Eq. 4a or 4b could return good fits but with $C$ and $D$ substantially different from 1.0, or, in the worst case, neither equation may fit the data.

The parameters $C$ and $D$ were assumed to be independent of time but they were fit separately for the San Jose and Davis data. We found that $C$ and $D$ were relatively insensitive to whether $A$ or $B$ (affecting the $Q_{sky}$ term) were allowed to vary monthly, as long as least one was allowed to vary. There were no statistically significant differences in the $C$ and $D$ values among any of the different possible fits that allowed $A$ or $B$, or both, to vary.

## Results

To test which of the two convective heat flow functions was better, fits were done for each month separately and for all months together. Equation 4b provided better fits for 13 of the 17 monthly data sets. Assuming a simple binomial probability model, this implies that there is a less than 0.5% chance that Eq. 4a provides as good or better fits than Eq. 4b, i.e, the results are statistically significant at the 0.5% level. Equation 4b also gave better fits when the monthly

[2] Fits and statistical analysis were done with the JMP statistical analysis package, version 3.0.

data were combined. The $R^2$ values for the fits with Eq. 4b were 93% for San Jose and 88% for Davis, compared to 92% and 87%, respectively, for Eq. 4a.

Table 6 shows the parameter values for the fits based on Eq. 4b. The coefficients $A$ and $B$ of the $Q_{sky}$ term are strongly correlated to each other. $< Q_{sky} >$, the average value of $Q_{sky}$, and $A + B < Q_{sky} >$, the linear fit from Eq. 2, were typically very close to each other. What differed was the amount of variation in $Q_{sky}$ as predicted by the unadjusted sky radiation algorithms and by the best linear fit to the data (Eq. 3). The average value of the offset term, $A$, was not significantly different from zero, but individual monthly values were significantly different from zero. This was consistent with our earlier comment that the $Q_{sky}$ algorithms may be correct on an annual basis, but may be substantially in error month by month.

**Table 6: Best-fit parameter values**

| Parameter | San Jose[a] | Davis[b] | Average | Standard Error |
|---|---|---|---|---|
| $A$ (W/m$^2$)[c] | 9.5 | -79 | -35 | 44 |
| $B$ | 0.93 | 1.19 | 1.06 | 0.18 |
| $C$ | 1.05 | 1.01 | 1.03 | 0.03 |
| $D$ | 1.65 | 1.67 | 1.66 | 0.02 |

a Brown's sky emissivity algorithm [BR97] was used for the San Jose data.

b Walton's sky emissivity algorithm [WA83] was used for the Davis data.

c Different values of $A$ were used for each month. The value shown is the average. The maximum and minimum $A$ values were 39 and -103, respectively.

Table 5 indicates that the natural convection parameter, $C$, and the forced convection parameter, $D$, are not significantly different between the two cities. The site-averaged value of $C$ is $1.03 \pm 0.03$; this is consistent with 1.0, which is the flat-plate value. We will therefore set the Nusselt number for natural convection with $\Delta T > 0$ to the flat-plate value, and we will indicate it as an average value over the roof surface since natural convection is expected to have negligible position dependence for horizontal roofs. This gives

$$\overline{Nu}_n = 0.15 Ra^{1/3} \text{ for } \Delta T > 0 \quad \text{[natural convection]} \tag{5a}$$

Since we see good agreement with the natural convection flat-plate correlation for $\Delta T > 0$, we will assume that the appropriate flat-plate correlation from Table 4 holds for $\Delta T < 0$ (which corresponds to downward heat flow). This gives

$$\overline{Nu}_n = 0.27 Ra^{1/4} \text{ for } \Delta T < 0 \quad \text{[natural convection]} \tag{5b}$$

The site-averaged value of $D$ is $1.66 \pm 0.02$; this is significantly higher than the flat-plate value of 1.0. An explanation for this is that the roughness of the roof surface increases the forced convection coefficient relative to the flat-plate values, which were determined for very smooth surfaces. To account for the effect of surface roughness, Walton [WA83, p. 73] has derived a roughness multiplier, $R_f$, from plots of surface heat transfer coefficient *vs* air velocity [AF97, p. 24.1] based on measurements of 0.3-m square surfaces with different roughness [RO37]. Table 7 show's Walton's $R_f$ values for different roughnesses, in order of increasing roughness.

**Table 7: Forced Convection Surface Roughness Multiplier**

| ASHRAE roughness number | Example surfaces with this roughness number | Forced convection multiplier, $R_f$ |
|---|---|---|
| 6 | Glass, paint on pine | 1.00 |
| 5 | Smooth plaster | 1.11 |
| 4 | Clear pine | 1.13 |
| 3 | Concrete | 1.52 |
| 2 | Brick, rough plaster | 1.67 |
| 1 | Stucco | 2.10 |

The granular capsheet surface finish corresponds to roughness 2, and the value of $D$, $1.66 \pm 0.02$, is consistent with the $R_f$ value of 1.67 for this roughness. We will therefore proceed by writing the Nusselt number for forced convection as

$$Nu_{f,x} = R_f\, 0.0296\, \mathrm{Re}_x^{4/5}\, \mathrm{Pr}^{1/3} \qquad \text{[forced convection, turbulent flow]} \tag{6}$$

Here $x$ is the distance, in the direction of flow, from the edge of the roof to the point that the Reynolds number is evaluated. (For a given point on the roof, $x$ will vary with wind direction). As noted earlier, our best fits assumed turbulent flow only, and Eq. 6 is applicable only to this condition.

If $x$ is in a region with laminar flow, the following equation should be used instead:

$$Nu_{f,x} = R_f\, 0.332\, \mathrm{Re}_x^{1/2}\, \mathrm{Pr}^{1/3} \qquad \text{[forced convection, laminar flow]}$$

Combining the expressions for natural convection (Eq. 5a,b) and forced convection (Eqs. 6 and 7) we obtain the equations for the convective heat transfer coefficient shown in Table 8. In this table $L_n$ is the characteristic length for natural convection, given by (roof area)/perimeter, and $x_c$ is the "critical length" for forced convection. If $x < x_c$, $x$ is in the laminar flow region; if $x > x_c$, $x$ is in the turbulent flow region (see Fig. 11). The critical length is given by

$$x_c = \mathrm{Re}_{x,c} \frac{\mu}{\rho w}$$

The standard value of $Re_{x,c}$ is $5 \times 10^5$ [IN96]. This value is based on laboratory measurements on small flat plates. However, real roofs differ from laboratory samples in that roofs are often rough surfaced, have protrusions (such as parapets) that promote turbulence, and, perhaps most importantly, are of sufficient size that natural convection is almost always turbulent for $\Delta T > 0$. We therefore treated $Re_{x,c}$ as a free parameter in our fits. Our best fits with $\Delta T > 0$ indicated that $Re_{x,c}$ was below 1000. If the air above the roof is turbulent because of natural convection—which is what we observe—then it should remain turbulent as wind speed increases and the roof transitions into the forced convection regime. This means that for $\Delta T > 0$ there is no laminar forced convection region and therefore $Re_{x,c} \approx 0$ (and, correspondingly, $x_c \approx 0$).

In the $\Delta T < 0$ case, natural convection does not produce turbulence. We have no usable data for $\Delta T < 0$ so we cannot judge the extent to which $Re_{x,c}$ should be less than the standard value of $5 \times 10^5$. In Table 8 we have used the standard value of $Re_{x,c}$ for $\Delta T < 0$, which gives $x_c = 5 \times 10^5 \mu/(\rho w)$.

**Table 8: Expressions for convective heat transfer coefficient at a point on the roof.**

| $\Delta T$ range | $x$ range | $h_x$ | | |
|---|---|---|---|---|
| $\Delta T \geq 0$ | $x \geq x_c \approx 0$ | $\eta \frac{k}{L_n} 0.15 Ra_{L_n}^{1/3} + \frac{k}{x} R_f 0.0296 \mathrm{Re}_x^{4/5} \mathrm{Pr}^{1/3}$ | Natural convection plus turbulent forced convection | (8a) |
| $\Delta T < 0$ | $x < x_c = 5\mathrm{x}10^5 \mu/(\rho w)$ | $\eta \frac{k}{L_n} 0.27 Ra_{L_n}^{1/4} + \frac{k}{x} R_f 0.332 \mathrm{Re}_x^{1/2} \mathrm{Pr}^{1/3}$ | Natural convection plus laminar forced convection | (8b) |
| | $x \geq x_c = 5\mathrm{x}10^5 \mu/(\rho w)$ | $\eta \frac{k}{L_n} 0.27 Ra_{L_n}^{1/4} + \frac{k}{x} R_f 0.0296 \mathrm{Re}_x^{4/5} \mathrm{Pr}^{1/3}$ | Natural convection plus turbulent forced convection | (8c) |

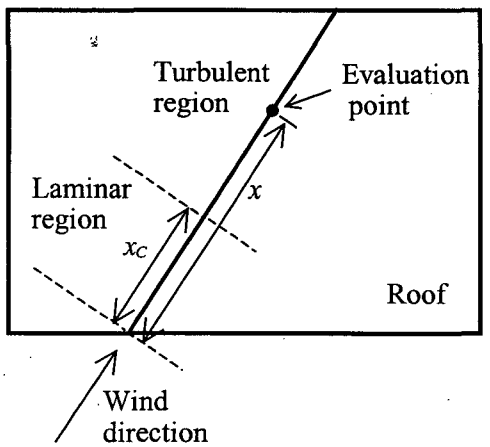


**Figure 11: Line along wind direction showing laminar and turbulent regions for forced convection. In this example the evaluation point for the heat transfer coefficient is in the turbulent region ($x > x_c$).**

***Application to building thermal analysis***

There are several approaches for using the expressions for $h_x$ in building thermal analysis programs. For programs that calculate heat transfer on a closely-spaced grid of points covering the roof, $h_x$ can be calculated at each grid point using Eqs. 8a-c. In this case, $x$ will depend on the roof geometry, the location of the grid point and the wind direction.

For the more common case in which the program calculates the *average* heat transfer for the entire roof, or for individual sections of the roof, an average value of $h_x$ for the roof or for each section is needed. This average value can be calculated for an arbitrarily-shaped roof, or for a section of the roof, by dividing the surface into thin strips along the wind direction, calculating the average heat transfer coefficient over each strip (as described below), and then calculating the length-weighted average of the strip values. Because this method is computationally intensive, we describe in the following two simplified methods for determining average heat transfer coefficients:

1. The "center-point method," in which the average coefficient for a roof section is approximated by the value at the center of the section.

2. The "wind-direction averaged method," in which the average coefficient for simple geometries, like circles and rectangles, is calculated by averaging over the surface for each wind direction and then averaging over all wind directions assuming a uniform distribution of wind directions.

***Heat transfer coefficient evaluated using center-point method***

A computationally-efficient method for computing the forced convection heat transfer coefficient for a section of roof is to evaluate the coefficient at the center point (center of gravity) of the section, as shown in Fig. 12, and to take the resulting value, $h_{f,center}$, as an approximation to the area-averaged value. This method overestimates the effective average length in the wind flow direction but the error is reduced by the fact that the forced convection heat transfer coefficient goes as an inverse fractional power of distance ($1/x^{1/2}$ for laminar flow and $1/x^{1/5}$ for turbulent flow).

*Center-point method applied to the entire surface of the roof*

The bias is largest when this method is applied to the entire roof surface. In this case, exact calculations for rectangular shapes show that for laminar flow $h_{f,center}$ underestimates the area-averaged value of the forced convection coefficient by 30% for flow normal to a side of the rectangle, and by 47% for flow along a diagonal of the rectangle. The error is considerably less for turbulent flow, where the forced convection coefficient is less sensitive to distance. In this case, $h_{f,center}$ underestimates the area-averaged value by only 8% to 17% for wind directions ranging from normal to a side of the rectangle to along a diagonal.

*Center-point method applied to a section of the roof*

We now consider the case in which the center-point method is applied to one of the sections in a multi-section roof. Figure 12 shows an example where the roof is divided into three sections. If the wind comes from the left in this figure, the center-point method gives a percentage error in the area-averaged coefficient for roof sections 1 and 2 that is identical to the percentage error for the whole roof surface. The error for roof section 3 will be smaller because the relative difference in flow distances from where the wind enters the section to where it leaves the section is much smaller than for sections 1 and 2.

Calculations show that the error declines rapidly as the size of the section declines relative to the length of the wind path over the roof. Consider, for example, a roof section that is half the lineal dimension of the roof. If this section is located where section 2 is in Fig. 12 and the wind flow is from the right or above, the error is 1.4% for laminar flow and 0.5% for turbulent flow. In comparison, for flow along the right-hand diagonal of the section, the error is 6.8% for laminar flow and 2.7% for turbulent flow.

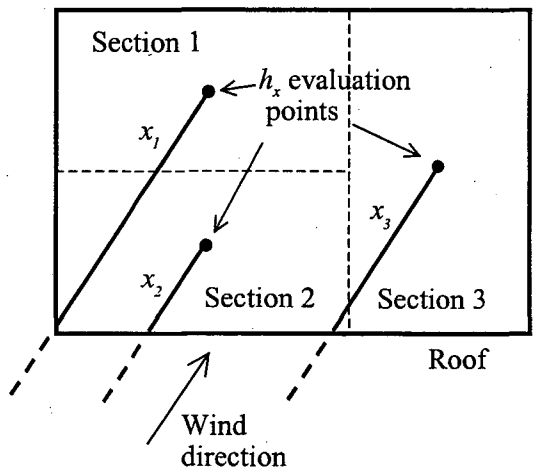


**Figure 12: Roof divided into three sections. For a given wind direction, the average heat transfer coefficient for each section is approximated by the value at the center of the section.**

***Heat transfer coefficient averaged over a strip along the wind direction***

Using the approach described in [IN96, p. 356], the average forced-convection Nusselt number over a strip of length $L$ along the wind direction (Fig. 13) can be calculated by integrating Eqs. 6 and 7 over the laminar and turbulent regions of the strip. This gives

$$\overline{Nu}_{f,strip} = R_f\left(0.037\,\mathrm{Re}_L^{4/5} - E\right)\mathrm{Pr}^{1/3} \quad \text{for } x_c < L \text{ (laminar and turbulent regions present)} \tag{9a}$$

$$= R_f\,0.664\,\mathrm{Re}_L^{1/2}\,\mathrm{Pr}^{1/3} \quad \text{for } x_c \geq L \text{ (only laminar region present)} \tag{9b}$$

The convective heat transfer coefficient averaged over a strip is then given by

$$\bar{h}_{strip} = \eta\frac{k}{L_n}\overline{Nu}_n + \frac{k}{L}\overline{Nu}_{f,strip}$$

Table 9 summarizes the expressions for the heat transfer coefficient averaged over a strip for different ranges of temperature difference and critical length.

In Eq. 9a the laminar correction, $E$, is given by

$$E = 0.037\,\mathrm{Re}_{x,c}^{4/5} - 0.664\,\mathrm{Re}_{x,c}^{1/2}$$

The standard value of $Re_{x,c}$ is $5\text{x}10^5$ [IN96]. This value is based on laboratory measurements on small, smooth flat plates. However, real roofs differ from laboratory samples in that they are often rough surfaced, have protrusions—such as parapets or rooftop equipment—that promote turbulence, and perhaps most importantly, are of sufficient size that natural convection is almost always turbulent for $\Delta T > 0$. We therefore treated $Re_{x,c}$ as a free parameter in our fits. Our best fits with $\Delta T > 0$ indicated that $Re_{x,c}$ was below 1000.

If the air above the roof is turbulent—which is what we observe—then it should remain turbulent as wind speed increases and the roof transitions into the forced convection regime. This means that there is no laminar forced convection region and, therefore, $Re_{x,c} = 0$ (and, correspondingly, $E = 0$ and $x_c = 0$).

For $\Delta T < 0$ natural convection does not produce turbulence. We have no useable data for $\Delta T < 0$ so we cannot judge the extent to which $Re_{x,c}$ in this case differs from standard value. Therefore, in Table 9, we have used the standard value for $\Delta T < 0$, which gives the factor $E = 871$ in Eq. 10c.

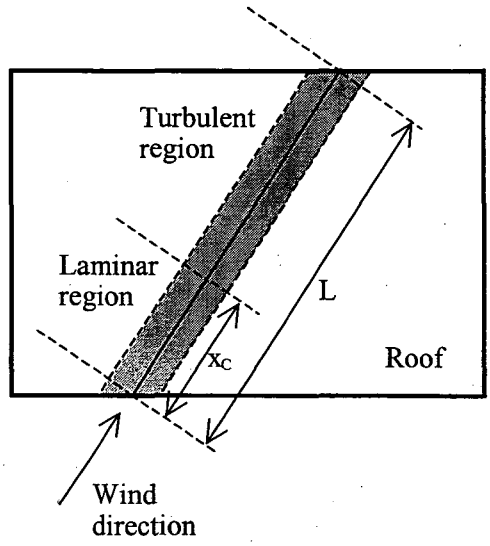


**Figure 13: Roof strip along wind direction showing laminar and turbulent regions.**

**Table 9: Expressions for convective heat transfer coefficient averaged over a strip of length *L*.**

| $\Delta T$ range | $L$ range | $\bar{h}_{strip}$ (averaged over a strip of length $L$) | |
|---|---|---|---|
| $\Delta T \geq 0$ | $L > x_c \approx 0$ | $\eta \frac{k}{L_n} 0.15 Ra_{L_n}^{1/3} + \frac{k}{L} R_f 0.037 \mathrm{Re}_L^{4/5} \mathrm{Pr}^{1/3}$ | (10a) |
| $\Delta T < 0$ | $L < x_c = 5\mathrm{x}10^5 \mu/(\rho w)$ | $\eta \frac{k}{L_n} 0.27 Ra_{L_n}^{1/4} + \frac{k}{L} R_f 0.664 \mathrm{Re}_L^{1/2} \mathrm{Pr}^{1/3}$ | (10b) |
| | $L \geq x_c = 5\mathrm{x}10^5 \mu/(\rho w)$ | $\eta \frac{k}{L_n} 0.27 Ra_{L_n}^{1/4} + \frac{k}{L} R_f (0.037 \mathrm{Re}_L^{4/5} - 871) \mathrm{Pr}^{1/3}$ | (10c) |

***Heat transfer coefficient averaged over surface area for a given wind direction***

For rectangles, the surface-averaged forced-convection heat transfer coefficient, $\bar{h}_f$, can be derived by dividing the roof into strips along the wind direction (Fig. 14), calculating the average coefficient over each strip (as described in the previous section), then averaging the contributions from all of the strips. The result can be expressed in terms of the center-point values described previously. For a rectangle of width $W$ and length $rW$ (with $r \geq 1$) $\bar{h}_f$ is given by the following expressions, where the incidence angle, $\theta$, is the angle between the wind direction and the short side of the rectangle (Fig. 14).

For $\tan\theta < r$:

$$\bar{h}_{f,lam} = h_{f,center,lam} \sqrt{2}(1 + \tan\theta / 3r) \qquad \text{[laminar flow]}$$

$$\bar{h}_{f,turb} = h_{f,center,lam} (5/36) 2^{-1/5} (9 + \tan\theta / r) \qquad \text{[turbulent flow]}$$

For $\tan\theta > r$:

$$\bar{h}_{f,lam} = h_{center,lam} \sqrt{2}(1 + 3r / \tan\theta) \qquad \text{[laminar flow]}$$

$$\bar{h}_{f,turb} = h_{center,lam} (5/36) 2^{-1/5} (9 + r / \tan\theta) \qquad \text{[turbulent flow]}$$

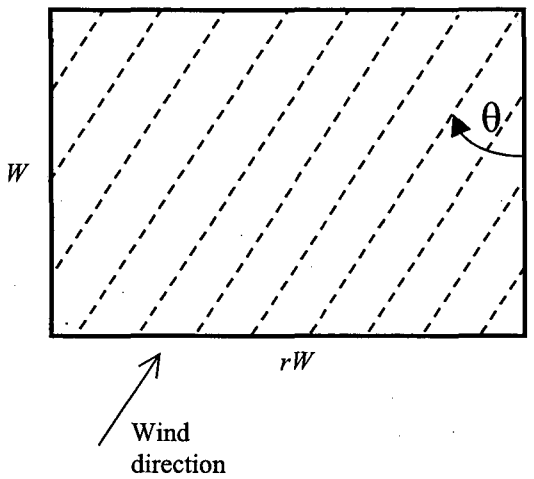


**Figure 14: Roof divided into strips along the wind direction.**

***Heat transfer coefficient averaged over roof area and wind direction***

In some cases the wind direction at a site may be sufficiently variable that it is appropriate to evaluate the average of the heat transfer coefficient over wind direction as well as area. In the following we have first calculated the surface average for each wind direction and then averaged the resulting values over wind direction assuming that all wind directions are equally probable. The result should only be applied to cases where the simulation time period is sufficiently long to incorporate a wide range of wind directions for a given wind speed.

The approach we have taken is to treat the average over surface area and wind direction in terms of an effective length, $L_{eff}$, and an effective critical length, $x_{c,eff}$, so that in Eqs. 10a-c $L$ is replaced by $L_{eff}$ and $x_c$ is replaced by $x_{c,eff}$, yielding Eqs. 11a-c in Table 10.

*Effective length*

For simple geometries (such as circles and rectangles) it is relatively easy to compute $L_{eff}$ for a uniform distribution of wind directions. When the shape is compact, such as for a circle or square, $L_{eff}$ is smaller than the nominal dimension of the surface. For example, for a circle of diameter $d$, $L_{eff} = 0.81d$ for laminar flow and $0.82d$ for turbulent flow. For a square of side $d$, $L_{eff} = 0.85d$ for laminar flow and $0.88d$ for turbulent flow.

For a rectangle of area, $A$, and perimeter, $P$, $L_{eff}$ can be approximated as follows:

$$L_{eff,lam} = (0.860 - 0.008t)l \qquad \text{[rectangle]}$$

$$L_{eff,turb} = (0.938 - 0.056t)l \qquad \text{[rectangle]}$$

where

$$l = 4A/P$$

$$t = 4\sqrt{A}/P$$

An approximation good to about 3% that can be used for either laminar or turbulent flow is

$$L_{eff} = (0.899 - 0.032t)l \qquad \text{[rectangle]}$$

When applied to a circle, this equation overestimates $L_{eff}$ by about 6%. This suggests that this equation can serve as a first approximation for convex shapes other than circles and rectangles. (We have not analyzed concave shapes, in which sections of the roof are separated by open areas, so we have no recommendation on the applicability of this equation for this class of shapes.)

*Effective critical length*

For mixed (laminar plus turbulent) flow, which applies when $\Delta T > 0$, we also have to calculate an effective critical length, $x_{c,eff}$. As $x_c$ approaches the maximum linear dimension[3], $L_{max}$, of the surface, $x_{c,eff}$ approaches $L_{eff}$. As $x_c$ approaches zero, $x_{c,eff}$ approaches a value slightly above $x_c$. For a circle the following equation is good to about 3%:

$$x_{c,eff} = x_c \frac{1.089 - 0.771s}{1.0 - 0.614s} \qquad \text{[circle]}$$

where $x_c \approx 5\text{x}10^5 \mu/(\rho w)$ and $s = x_c/(\text{diameter of circle})$.

For a rectangle of width $W$ and length $rW$ ($r \geq 1$) the following expressions for $x_{c,eff}$ are good to about 6%:

$$\text{For } x_c \leq W, \quad x_{c,eff} = x_c \left( \frac{0.096 + 0.941r}{1 + 0.777r} \right) \left( \frac{1 + r - 0.589 \frac{x_c}{W}}{r} \right) \qquad \text{[rectangle]}$$

where $x_c \approx 5\text{x}10^5 \mu/(\rho w)$. In this case, $x_{c,eff} \approx x_c$.

$$\text{For } x_c > W, \quad x_{c,eff} = W \left( \frac{0.85 + 0.075r - 0.655z + 4.248zr}{1 + 0.046r + 1.915z + 2.371zr} \right) \qquad \text{[rectangle]}$$

with

$$z = \frac{\frac{x_c}{W} - 1}{\left(1 + r^2\right)^{1/2} - 1}$$

In this case, $x_{c,eff} \approx W$.

The final expressions for the wind-direction-averaged, surface-averaged convective heat transfer coefficient for a rectangular roof are given in Table 10.

[3] For a circle the maximum lineal dimension is the diameter; for a rectangle it is the diagonal.

**Table 10: Expressions for convective heat transfer coefficient averaged over surface area and wind direction for a rectangular or circular roof.**

| $\Delta T$ range | Range of maximum lineal dimension, $L_{max}$ | $\bar{h}$ (averaged over rectangular roof surface and wind direction) |
|---|---|---|
| $\Delta T \geq 0$ | $L_{max} > x_{c,eff} \approx 0$ | $\eta \frac{k}{L_n} 0.15 Ra_{L_n}^{1/3} + \frac{k}{L_{eff}} R_f 0.037 \mathrm{Re}_{L_{eff}}^{4/5} \mathrm{Pr}^{1/3}$ (11a) |
| $\Delta T < 0$ | $L_{max} < x_{c,eff}$ | $\eta \frac{k}{L_n} 0.27 Ra_{L_n}^{1/4} + \frac{k}{L_{eff}} R_f 0.664 \mathrm{Re}_{L_{eff}}^{1/2} \mathrm{Pr}^{1/3}$ (11b) |
| | $L_{max} \geq x_{c,eff}$ | $\eta \frac{k}{L_n} 0.27 Ra_{L_n}^{1/4} + \frac{k}{L_{eff}} R_f \left[ 0.037(\mathrm{Re}_{L_{eff}}^{4/5} - \mathrm{Re}_{x_{c,eff}}^{4/5}) + 0.664 \mathrm{Re}_{x_{c,eff}}^{1/2} \right] \mathrm{Pr}^{1/3}$ (11c) |

## Discussion

In our analysis, measured heat flows were fit to a function of wind speed and temperature difference. For the July 1996 Davis data, Fig. 15 shows the residual error in $h$ resulting from this fit plotted as $h_{meas} - h_{fit}$ vs. $h_{fit}$, where $h_{meas}$ is the measured value of $h$ calculated from Eq. 1 and $h_{fit}$ is the fitted value of $h$ obtained from Eq. 4b using the average fitted parameters in Table 6. (Seven extreme residuals are not shown in this plot in order to keep the detail at high values of $h$ visible). Two comments are in order here.

First, although our interest is in $h$, the actual fits are to net heat flow, $Q_{net}$, defined as $Q_{solar}+Q_{cond}-Q_{IR}$ (see Eq. 3). Figure 16 shows the residual error in $Q_{net}$, i.e., $Q_{net,meas}-Q_{net,fit}$, vs. $Q_{net,fit}$. These residuals do not show the extreme behavior found for $h$ in Fig. 15. It is important to note that the abscissa in Figs. 15 and 16 shows the fitted values, and that these values cover a physically reasonable range. The measured $Q_{net}$ values also cover a physically reasonable range, which is why the residuals are relatively small. However, convective flows, and thus the convective heat transfer coefficient, were computed as the difference between $Q_{net}$ and $Q_{sky}$. The few percent of the residuals in Fig. 15 that are large show that this procedure sometimes results in unphysical estimates of these heat flows. Because of this, fits have to be based on $Q_{net}$ and not on $h\Delta T$.

Second, the fit used in generating Figs. 15 and 16 uses the average fitted parameters from Table 6. For the month shown, there is a distinct bias in the residual error (systematically negative values) for the largest fitted $h$ and $Q_{net}$ values ($h_{fit} > 12$, $Q_{net} > 0$). Other monthly plots (not shown) demonstrate that this bias varies from month to month. The clue to this behavior is that for any individual month there are only a small number of points with large $h_{fit}$ (or large $Q_{net}$). Figure 17 shows the data for a typical month. For this month all the large $h_{fit}$ values occurred on one day (the 19$^{th}$). This day did not have unusually high wind speeds. This day also had high values of $Q_{net}$, and in general we found that there would be one or two days in each month with atypically high values of $h_{fit}$ and $Q_{net}$. As previously noted, $Q_{sky}$ had to be adjusted at least monthly to get reasonable fits. However, any particular day may vary from the monthly average. In regions of the fit with many data points these variations will average out. But in regions of the fit with limited data, such as $h_{fit} > 12$ in Fig. 15 or $Q_{net} > 0$ in Fig. 16, the day-to-day variation is not removed by averaging, resulting in a bias deviation from the overall average fit.

### Limitations and Applicability

Our expressions for $h$ are applicable in the following situations:

1. The roof is horizontal. However, it is probably safe to use the correlation for roof tilts up to about $20^0$. In no case should it be applied to vertical walls.
2. The roof is dry. The correlations should not be used when it is raining or when condensation is likely (surface temperature below dewpoint temperature).
3. The roof surface is flat and relatively unobstructed, i.e., at most a few percent of the roof area has protrusions like vents, roof-top equipment, etc.; the height of the roof parapet, if present, is only a few percent of the roof dimensions; and the roof surface is not in the wind shadow of another part of the building.

## Conclusions

The correlation for outside convective air film coefficient that we have determined should lead to more accurate roof heat transfer calculations when used in building thermal simulation programs.

A major limitation in our analysis was lack of sky long-wave radiation measurements. The use of sky emissivity models restricted our analysis to a subset of the data and reduced the precision of the fits. We recommend that on-site meteorological measurements include horizontal sky long-wave irradiance whenever building envelope thermal measurements are made.

Our results indicated that flat roofs of the size typical of most commercial buildings produced turbulence under almost all conditions. We confirmed that the standard flat-plate model for turbulent natural convection model correlated well with our measured convective heat flows. The standard flat-plate model for forced convection model also correlated well, but only after scaling by a factor of about 1.6 that we attributed to the roughness of the roof surface.

Additional studies are recommended to extend the correlation to tilted roofs. It would also be useful to measure the effects of roof condensation and rain on surface heat transfer, and to verify the applicability of a surface roughness multiplier.

## Acknowledgments

We thank Steve Konopacki and Hashem Akbari of Heat Island Group at Lawrence Berkeley National Laboratory and Leo Rainer of the Davis Energy Group for their assistance.

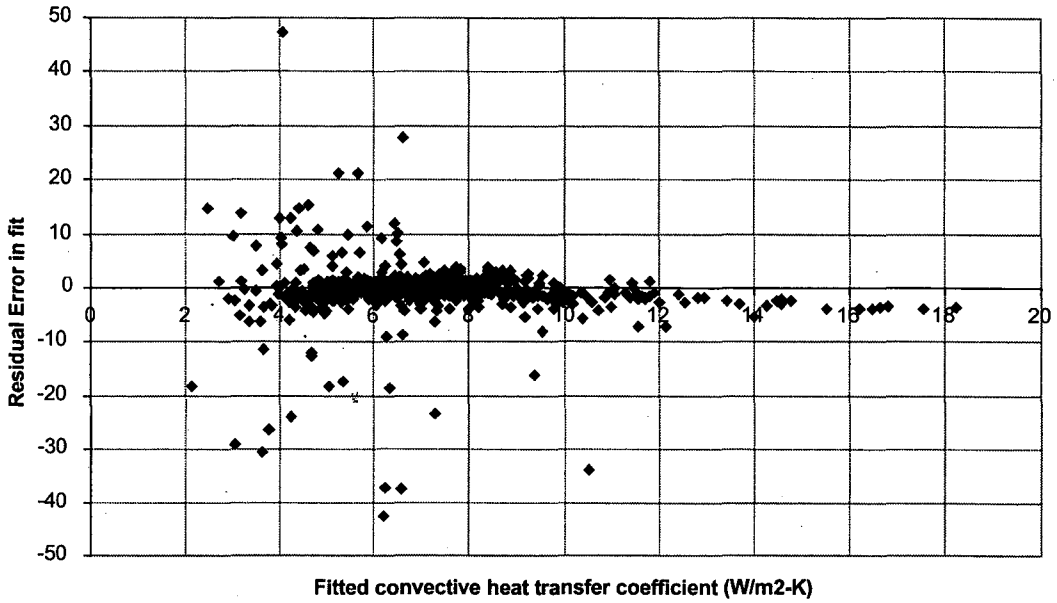


**Figure 15:** **Residual error in the fitted convective heat transfer coefficient at roof center *vs* the fitted convective heat transfer coefficient for the data shown in Fig. 7.**

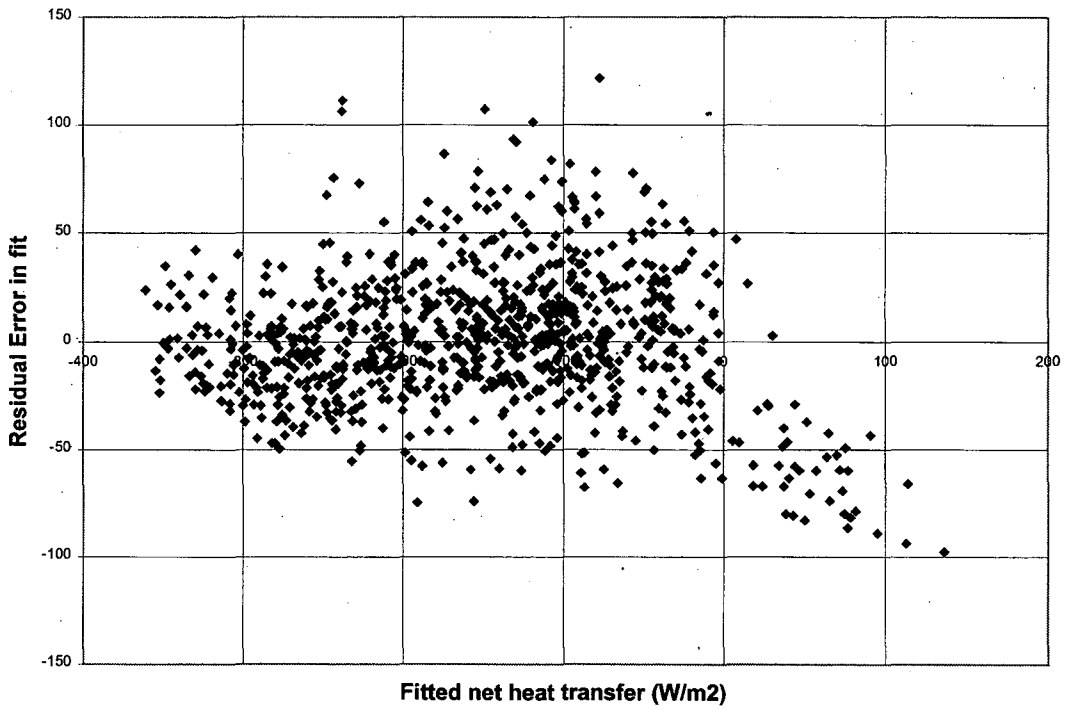


**Figure 16:** **Residual error in fitted net heat transfer at roof center *vs* the fitted net heat transfer for the data shown in Fig. 7.**

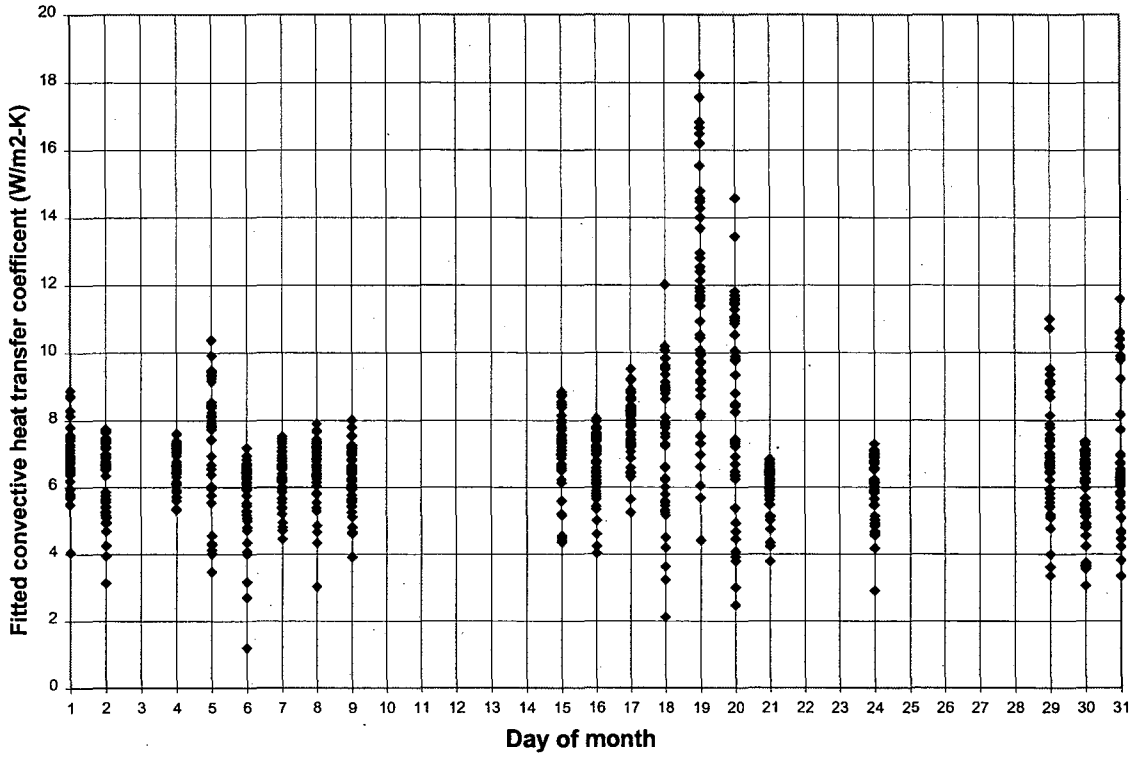


**Figure 17: Fitted convective heat transfer coefficient *vs* day of month for the data shown in Fig. 7.**

## References


AF97 "ASHRAE Handbook of Fundamentals," American Society of Heating, Refrigeration and Air-Conditioning Engineers, 1997.

BR97 Brown, D., "An improved meteorology for characterizing atmospheric boundary layer turbulence dispersion". Ph.D. Thesis, Department of Mechanical and Industrial Engineering, University of Illinois at Urbana-Champaign, 1997.

CA59 Carslaw, H.S., and Jaeger, J.C., "Conduction of Heat in Solids," Oxford University Press, London, 1959.

CI73 CIE, "Standardization of Luminance Distribution on Clear Skies", CIE Publication No. 22, 1973.

GO73 Goldstein, R.J., Sparrow, E.M, and Jones, D.C., "Natural Convection Mass Transfer Adjacent to Horizontal Plates," Int. J. Heat and Mass Transfer, 16, 1025, 1973.

IN96 Incropera, F., and DeWitt, D., "Fundamentals of Heat and Mass Transfer," Fourth Edition, John Wiley & Sons, New York, 1996.

KO98 Konopacki, S., et. al., "Demonstration of Energy Savings of Cool Roofs." Lawrence Berkeley National Laboratory report LBNL-40673, 1998.

MA84 Martin M., and Berdahl, P., "Characteristics of infrared sky radiation in the United States," Solar Energy 33, 321-336 (1984).

RO30 Rowley, F.B., Algren, A.B., and Blackshaw, J.L., "Surface Conductances as Affected by Air Velocity, Temperature and Character of Surface," ASHVE Trans. 36, 429 (1930).

SC70 Schulze, R. W., "Strahlenlima der Erde," Steinkopff Verlag, Darmstadt, 1970.

WA83 Walton, G. N., "Thermal Analysis Research Program Reference Manual," NBSIR 83-2655, National Bureau of Standards, Washington, DC 20234.

YA94 Yazdanian, M., and Klems, J., "Measurement of the Exterior Convective Film Coefficient for Windows in Low-Rise Buildings," ASHRAE Trans. 100, Pt. 1, 1087-1096, 1994.

## Appendix A: Sky Emissivity Models

Sky emissivity models by Walton [WA83], Martin and Berdahl [MA84], and Brown [BR97] were used to estimate the long-wave radiation from the sky incident on the roof. In Davis the best fits were obtained with the Walton model, while in San Jose the best fits were obtained with the Brown model. The three sky emissivity models are summarized below.

The sky long-wave radiation incident on the roof is given by

$$Q_{sky} = \sigma \varepsilon_{sky} T_a^4$$

where σ is the Stefan-Boltzmann constant (5.669 x $10^{-8}$ W/$m^2$), $T_a$ is the outside air temperature (K), and $\varepsilon_{sky}$ is the effective sky emissivity, as given by the one of following three models for clear sky conditions:

$$\varepsilon_{sky}(\text{Walton}) = 0.787 + 0.764 \ln(T_d / 273)$$

where $T_d$ = dewpoint temperature (K).

$$\varepsilon_{sky}(\text{Martin \& Berdahl}) = 0.711 + 0.01T_1(0.56 + 0.73T_1)$$

where $T_1 = 0.01(T_d\text{-}273)$.

$$\varepsilon_{sky}(\text{Brown}) = 0.65 + 0.41P_v^{0.9} \exp\left(\sum_{i=1}^{3} A_i (T_a - 240)^i\right)$$

where $A_1$ = -0.0103, $A_2$ = -6.1 x$10^{-4}$, $A_3$ = 6.1 x$10^{-6}$ and $P_v$ is in kPa.

## Appendix B: Air Properties

A number of air properties are needed for the calculation of the Grashof, Rayleigh and Reynolds numbers. These properties were calculated from least-squares fits to values from [AF97].

$Pr$ = Prandtl number = 0.96573 -1.5325 x$10^{-3}$ $T_f$ + 2.2746 x$10^{-6}$ $T_f^2$

where $T_f$ is the "film temperature" (K), calculated as the average of the surface temperature and outside air temperature.

$\mu$ = viscosity = -1.40695 x$10^{-7}$ + 7.7138 x$10^{-8}$ $T_f$ - 4.9903 x$10^{-11}$ $T_f^2$ (N-s/$m^2$)

$k$ = conductivity = -5.2344x$10^{-3}$ + 1.3511x$10^{-4}$ $T_f$ -1.0168x$10^{-7}$ $T_f^2$ (W/m-K)

$\rho$ = density = $(1 + \omega)/(1/\rho_{da} + \omega/\rho_{wv})$ (kg/$m^3$)

where

$\omega$ = humidity ratio = $0.62198P_v/(101.325 - P_v)$

$P_v$ = water vapor pressure (kPa)

$\rho_{wv}$ = density of water vapor = $252.398/T_f$ - 0.22113 + 3.8083 x$10^{-4}T_f$ (kg/$m^3$)

$\rho_{da}$ = $(359.757 - 0.053481T_f + 1.44323 \times 10^{-4} T_f^2 - 1.34123 \times 10^{-7} T_f^3)/T_f$ (kg/$m^3$)

Ernest Orlando Lawrence Berkeley National Laboratory
One Cyclotron Road | Berkeley, California 94720

Prepared for the U.S. Department of Energy under Contract No. DE-AC03-76SF00098